Quantification of Myocardial Perfusion in Human Subjects Using ^{82}Rb and Wavelet-Based Noise Reduction

Jou-Wei Lin, Robert R. Sciacca, Ru-Ling Chou, Andrew F. Laine, and Steven R. Bergmann

Division of Cardiology, Department of Medicine, and Department of Radiology, College of Physicians and Surgeons, Columbia University, New York; and Department of Biomedical Engineering, Columbia University, New York, New York

Quantification of myocardial perfusion with ^{82}Rb has been difficult to achieve because of the low signal-to-noise ratio of the dynamic data curves. This study evaluated the accuracy of flow estimates after the application of a novel multidimensional wavelet-based noise-reduction protocol. **Methods:** Myocardial perfusion was estimated using ^{82}Rb and a two-compartment model from dynamic PET scans on 11 healthy volunteers at rest and after hyperemic stress with dipyridamole. Midventricular planes were divided into eight regions of interest, and a wavelet transform protocol was applied to images and time–activity curves. Flow estimates without and with the wavelet approach were compared with those obtained using $H_2{}^{15}O$. **Results:** Over a wide flow range (0.45–2.75 mL/g/min), flow achieved with the wavelet approach correlated extremely closely with values obtained with $H_2{}^{15}O$ ($y = 1.03 \times -0.12$; $n = 23$ studies, $r = 0.94$, $P < 0.001$). If the wavelet noise-reduction technique was not used, the correlation was less strong ($y = 1.11 \times + 0.24$; $n = 23$ studies, $r = 0.79$, $P < 0.001$). In addition, the wavelet approach reduced the regional variation from 75% to 12% and from 62% to 11% ($P < 0.001$ for each comparison) for resting and stress studies, respectively. **Conclusion:** The use of a wavelet protocol allows near-optimal noise reduction, markedly enhances the physiologic flow signal within the PET images, and enables accurate measurement of myocardial perfusion with ^{82}Rb in human subjects over a wide range of flows.

Key Words: PET; rubidium; myocardial perfusion; wavelets

J Nucl Med 2001; 42:201–208

Quantification of myocardial perfusion is of paramount importance for the detection of ischemic heart disease and for the evaluation of therapeutic interventions. PET provides a noninvasive approach to quantify regional myocardial perfusion and perfusion reserve because of its ability to delineate the distribution of positron-emitting radionuclides within the myocardium. PET has been shown to accurately detect coronary artery disease with the cyclotron-produced flow tracers $^{13}NH_3$ (*1*) and $H_2{}^{15}O$ (*2*,*3*) as well as with generator-produced ^{82}Rb chloride (*4*,*5*) or ^{62}Cu-pyruvaldehyde bis(N^4-methylthiosemicarbazone) (*6*).

^{82}Rb is an attractive flow tracer because it is generator produced and has a short physical half-life ($t_{1/2}$, 76 s). The use of ^{82}Rb obviates the necessity of a cyclotron and reduces the time to perform sequential imaging in patient studies. Cardiac PET with ^{82}Rb has been used widely in clinical settings to diagnose coronary artery disease and to assess qualitatively the severity of coronary stenosis. Visual analysis of myocardial images has been reported to have a sensitivity of 87% and a specificity of 88% (*7*). However, accurate quantification of regional myocardial perfusion in absolute terms (i.e., mL/g/min) using PET and ^{82}Rb has been difficult to achieve because of the complex behavior of this tracer in the myocardium (*5*). Similar to other cationic tracers (e.g., $^{13}NH_3$), ^{82}Rb is partially extracted by the myocardium during a single capillary pass (*8*), but the extraction fraction varies inversely and nonlinearly with flow (*9*,*10*). Herrero et al. (*5*) measured myocardial perfusion in dogs using the relationship between flow and extraction fraction empirically derived from the experimental results of Goldstein et al. (*11*) and Mullani et al. (*9*,*10*). This approach was found to be insensitive to hyperemic flows >2 mL/g/min and may not be accurate for regions with prolonged ischemia or reperfusion (*4*). However, even when flow and extraction fraction were decoupled directly using a compartment model, estimates of blood flow were not accurate at hyperemic flows, and regional variation was high (*5*). Therefore, the quantification of myocardial perfusion with ^{82}Rb and dynamic PET in absolute terms has been limited.

The goal of this study was to evaluate the effect of using a wavelet-based noise-reduction protocol on improving the signal-to-noise ratio of time–activity curves derived from dynamic PET images with ^{82}Rb and, consequently, on improving the accuracy of quantification of myocardial perfusion with this tracer.

The wavelet transform is a newly developed signal-processing tool that decomposes a signal into different levels of resolution. A wavelet is a small wave that can be used to

Received Apr. 10, 2000; revision accepted Sep. 14, 2000.

For correspondence or reprints contact: Steven R. Bergmann, MD, PhD, Division of Cardiology, College of Physicians and Surgeons, Columbia University, PH 10-405, 630 W. 168th St., New York, NY 10032.

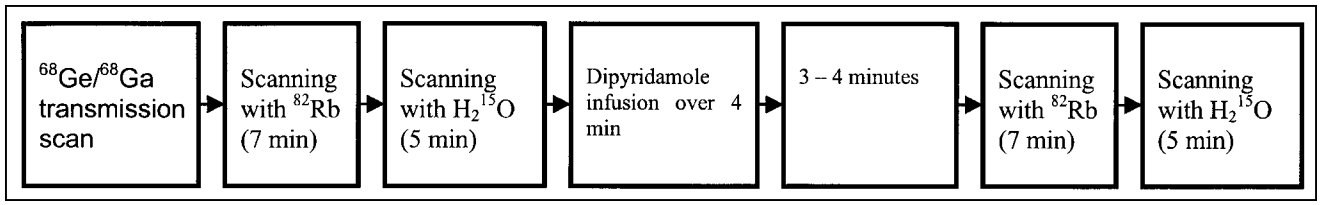

FIGURE 1. Imaging protocol. Each subject had a transmission scan followed by emission scans at rest with ^{82}Rb and $H_2{}^{15}O$. Dipyridamole was infused to induce hyperemia. Another set of emission images was obtained starting 3–4 min after end of dipyridamole administration.

represent simultaneously the time and frequency components of a signal. Wavelet-based noise reduction has the characteristics of optimally separating signal and noise, preserving the rapid rises and falls of a signal, and reconstructing a smooth signal from noise-imposed observations. Although the short half-life of ^{82}Rb is an attractive factor in reducing the time to acquire sequential scans, it also results in images with low signal-to-noise ratios. Thus, blood and myocardial time–activity curves are disrupted by inherent noise. Wavelet-based noise reduction provides a potential approach to objectively restore the true signal hidden within multidimensional images and therefore to enable accurate quantification of myocardial perfusion using ^{82}Rb in human subjects.

MATERIALS AND METHODS

Subjects

This study was approved by the institutional review board of the Columbia-Presbyterian Medical Center. Informed consent was obtained. Eleven healthy volunteers (5 men, 6 women; mean age, 44 y; age range, 24–70 y) without a history of ischemic heart disease were recruited. Seven subjects (3 men, 4 women) repeated the same scanning protocol in the following month.

Tomographic Data Acquisition

Each subject was placed in an ECAT EXACT-47 whole-body PET scanner (CTI/Siemens, Knoxville, TN). A transmission scan using an external ring of ^{68}Ge/^{68}Ga was obtained for attenuation correction. A dose of ^{82}Rb (average, 0.01 MBq/kg) was infused through an antecubital vein using the Bracco infusion system (Bracco Diagnostics, Princeton, NJ). A 7-min emission scan was acquired. After decay of radioactivity to background levels (^{82}Rb $t_{1/2}$, 76 s), a bolus of $H_2{}^{15}O$ (average, 0.008 MBq/kg) was administered intravenously and a 5-min scan was obtained. The doses were selected so that the system dead time was $<$30%. All subjects were then given 0.14 mg/kg/min dipyridamole intravenously over 4 min. Three minutes after the end of dipyridamole infusion, the same sequence of emission scans with ^{82}Rb and $H_2{}^{15}O$ was repeated (Fig. 1). Hemodynamic data, including heart rate, systolic blood pressure, and diastolic blood pressure, were recorded at the onset of the transmission scan, the beginning and end of each emission scan, and each minute during dipyridamole infusion. The sequence of scans was selected so that the shortest half-life tracer (^{82}Rb) was administered first and radioactivity had declined to near background levels before administration of $H_2{}^{15}O$.

Because of technical problems, such as generator failure and adverse response to dipyridamole, some subjects did not complete the scanning protocol. Thirteen successful pairs of ^{82}Rb–$H_2{}^{15}O$ studies at rest and 10 pairs at hyperemia (23 studies, total) were obtained.

Analysis of Tomographic Data

Emission data obtained after administration of ^{82}Rb were reconstructed into thirty-six 5-s frames, eight 15-s frames, and four 30-s frames (48 frames in 7 min). Data obtained after administration of $H_2{}^{15}O$ were reconstructed into twenty-four 5-s frames, six 10-s frames, and eight 15-s frames (38 frames in 5 min). The reconstructed data were reoriented to short-axis images, and the contour of the heart was delineated by the circumferential analysis (*12*). Myocardial tissue in each midventricular plane was divided into eight regions of interest (ROIs), each representing a volume of 0.70–0.85 cm^3. Forty to 64 ROIs were analyzed for each subject on the basis of the size of the heart (i.e., five to eight short-axis planes per subject). The arterial blood time–activity curves, necessary to define the input function, were selected from multiple pixels located near the center of the left ventricular chamber from basal slices. Forty to 64 ROIs were analyzed for each subject on the basis of the size of the heart.

Quantification of Myocardial Perfusion Using ^{82}Rb

Tissue and blood time–activity curves derived from dynamic PET images obtained after administration of ^{82}Rb were fitted to a previously developed two-compartment model (*5*). Myocardial perfusion was estimated for each ROI. This model estimates the forward and the backward rates of transport (k_1 and k_2) between the extracellular space and the intracellular space (Fig. 2). In addition to flow, k_1 and k_2, blood-to-tissue spillover fraction (F_{BM}) was estimated by the fitting process. The recovery coefficient (F_{MM}) was set to 0.65, and the fractional volume of the first compartment (Vd) was fixed at 0.75 mL/mL (*5*). For each subject, values of each ROI were analyzed separately and also averaged to get a global flow. The coefficient of variation (COV) (i.e., the inverse of the ratio of the global flow to the associated SD) was calculated. The approach used to quantify myocardial perfusion with unmodified raw data was referred to as the original protocol.

Quantification of Myocardial Perfusion Using ^{82}Rb Through Wavelet-Based Noise Reduction

A wavelet-based noise-reduction protocol was designed to restore the underlying multidimensional signal hidden within noise-imposed ^{82}Rb data. The bases of the wavelet transform were a set of spline-derived functions developed by Laine and Koren (*13*). The noise-reduction algorithm proposed by Donoho and Johnstone (*14–16*) and implemented by Lin et al. (*17*) for dynamic PET data evaluated local signals in the wavelet domain and ensured a near-optimal suppression of noise.

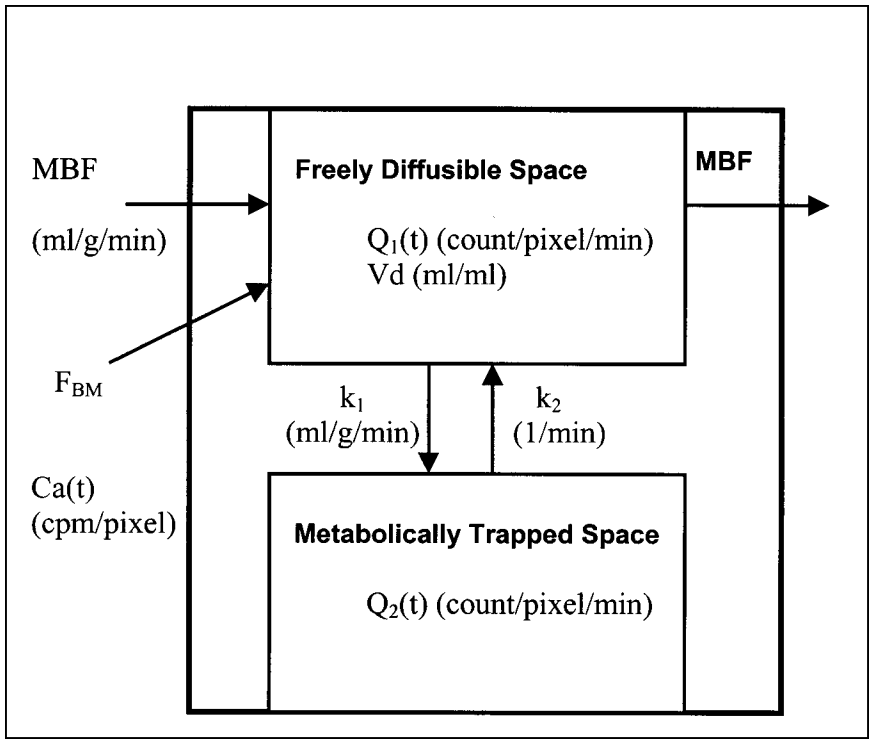

FIGURE 2. Two-compartment model describes kinetic behavior of ^{82}Rb in myocardium. $Q_1(t)$ and $Q_2(t)$ = ^{82}Rb activity in extracellular (intravascular and interstitial) and intracellular spaces, respectively; MBF = myocardial blood flow; k_1 and k_2 = forward and backward rates of transport between two compartments; Vd = distribution volume of free ^{82}Rb in myocardium; F_{BM} = spillover fraction from myocardial blood pool to myocardial tissue; Ca(t) = radioactivity in blood pool.

Each short-axis image of sequential ^{82}Rb frames in each midventricular plane underwent a two-dimensional wavelet-based noise reduction. The same ROIs were placed on the noise-suppressed images according to the coordinates determined in the circumferential analysis. The radioactivity in each ROI was averaged, and a tissue time–activity curve was then created. The tissue curves of adjacent ROIs on the same horizontal plane and those of the vertical stacks represent the time-varying radioactivity of the entire heart. The wavelet-based noise-suppression method was then applied to the spatial domain and the temporal domain of these dynamic curves to remove the noise that disrupted the continuity among adjacent ROIs and among sequential frames.

After the multidimensional noise-suppression process, a reconstructed tissue time–activity curve was created for each ROI. The blood curve found in the original approach also underwent a one-dimensional wavelet-based noise reduction. The blood curve and tissue curves were then fitted to the two-compartment model (Fig. 2) to obtain flow estimates.

Quantification of Myocardial Perfusion Using $H_2^{15}O$

Tissue and blood time–activity data derived from dynamic PET images obtained after administration of $H_2^{15}O$ were fitted to a previously developed and validated one-compartment model (*2*,*3*). Regional myocardial perfusion for each ROI was estimated. This model also estimated the F_{MM} and F_{BM} (*2*,*3*). Quantification of myocardial flow with $H_2^{15}O$ was used as a reference value, and estimates obtained from dynamic images with ^{82}Rb were compared with those from $H_2^{15}O$.

Statistics

A paired *t* test was used to compare hemodynamic data from the ^{82}Rb scans and $H_2^{15}O$ scans and also differences before and after pharmacologic stress. Pearson's correlation was calculated between the global flows derived from $H_2^{15}O$ images and those obtained with ^{82}Rb. An F test was used to determine whether the relationship between these two flow measurements differed significantly from the line of identity.

RESULTS

Hemodynamic Data of Subjects

The hemodynamic data for all subjects before and after pharmacologic stress are shown in Table 1. Heart rate, systolic blood pressure, diastolic blood pressure, and mean arterial pressure did not differ between resting ^{82}Rb and $H_2^{15}O$ scans. Heart rate and systolic blood pressure increased significantly after administration of dipyridamole. The time between ^{82}Rb and $H_2^{15}O$ administration after dipyridamole was 7–8 min. After dipyridamole, heart rate at the beginning of ^{82}Rb infusion was slightly higher (by 6 beats/min) than that at the time of injection of $H_2^{15}O$ ($P < 0.001$) because of the delay between the two scans. Systolic, diastolic, and mean arterial pressures did not differ.

Myocardial Images

The reconstructed midventricular short-axis images from the last 30-s frame obtained in a healthy subject after the administration of ^{82}Rb before and after wavelet-based noise reduction are shown in Figure 3. After the noise-reduction maneuver, the contour of the left ventricle became clearer.

Time–Activity Data Before and After Wavelet-Based Noise Reduction

Figure 4 shows ^{82}Rb time–activity curves from an ROI of a healthy volunteer studied at rest. The raw blood curve and the tissue curve are noisy and deviate from theoretic shapes

TABLE 1
Hemodynamics for Healthy Volunteers During PET Studies

Volunteer no.	RB1				HO1				RB2				HO2			
	HR	SBP	DBP	MAP	HR	SBP	DBP	MAP	HR	SBP	DBP	MAP	HR	SBP	DBP	MAP
1	63	82	44	57	63	86	58	67	81	92	52	65	83	92	56	68
2	51	96	54	68	51	96	54	68	98	108	52	71	85	113	55	74
3	59	132	72	92	58	116	74	88	80	126	80	95	75	129	80	96
4	64	106	58	74	66	102	56	71	91	108	62	77	81	110	58	75
5	59	113	53	73	66	112	54	73	99	131	68	89	92	128	60	83
6	61	119	71	87	65	121	64	83	98	125	70	88	97	124	68	87
7	73	132	79	97	83	132	65	87	93	144	60	88	93	150	65	93
8	74	118	68	85	73	120	70	87	83	118	66	83	82	120	69	86
9	69	136	78	97	69	136	78	97	98	130	78	95	84	140	83	102
10	63	137	61	86	55	146	70	95	89	144	64	91	88	146	64	91
11	41	98	52	67	42	96	50	65	70	101	49	66	57	101	50	67
Mean ± SD	62 ± 9	115 ± 18	63 ± 12	80 ± 13	63 ± 11	115 ± 19	63 ± 9	80 ± 12	89 ± 10*	121 ± 17*	64 ± 10	83 ± 11	83 ± 11*†	123 ± 18*	64 ± 10	84 ± 12

*$P < 0.05$ for comparison between resting and hyperemic studies on each hemodynamic measurement.
†$P < 0.05$ for comparison between $H_2{}^{15}O$ and ^{82}Rb scans on each hemodynamic measurement.
HR = heart rate (beats/min); SBP = systolic blood pressure (mm Hg); DBP = diastolic blood pressure (mm Hg); MAP = mean arterial pressure (mm Hg).
RB1 and RB2 represent ^{82}Rb studies before and after dipyridamole administration; HO1 and HO2 represent $H_2{}^{15}O$ studies. Administration of dipyridamole significantly increased heart rate and systolic blood pressure. Heart rate of HO2 was slightly lower than that of RB2.

FIGURE 3. Myocardial short-axis images obtained from last 30-s frame after administration of ^{82}Rb before (A) and after (B) wavelet-based noise reduction. Contour of heart became clearer and homogeneity of tissue counts increased after wavelet processing.

because of noise (Fig. 4A). Figure 4B shows the blood and tissue time–activity curves of the same region after the wavelet-based noise reduction.

Myocardial Blood Flow

The accuracy of the flow estimates obtained with ^{82}Rb before and after wavelet-based noise reduction was compared with the reference values derived from $H_2{}^{15}O$. Flow derived from $H_2{}^{15}O$ studied at rest was 0.92 ± 0.19 mL/g/min. The corresponding resting flow obtained from ^{82}Rb studies was somewhat higher (1.15 ± 0.46 mL/g/min) using the original protocol and was slightly lower (0.82 ± 0.26 mL/g/min) using the wavelet protocol. The correlation with the reference values of $H_2{}^{15}O$ was 0.66 ($P = 0.014$) and 0.92 ($P < 0.001$), respectively. The hyperemic flow derived from $H_2{}^{15}O$ was 1.89 ± 0.50 mL/g/min compared with 2.50 ± 0.54 mL/g/min ($r = 0.28$, $P = 0.418$) derived from ^{82}Rb studies before and 1.85 ± 0.56 mL/g/min ($r = 0.82$, $P = 0.003$) after wavelet-based noise reduction.

Figure 5 shows scatter plots of global flows obtained from ^{82}Rb and $H_2{}^{15}O$ combining resting and hyperemic studies ($n = 23$ studies). The linearity was poor when the original protocol was used (Fig. 5A: $y = 1.11 \times + 0.24$; $n = 23$, $r = 0.79$, $P < 0.001$). Some data points are located far above the regression line, indicating a poor correlation at high flows. The correlation and linearity were significantly improved after the wavelet protocol was applied (Fig. 5B: $y = 1.03–0.12$; $r = 0.94$, $P < 0.001$).

An F test was used to evaluate whether these two measurements yielded identical values ($F = 1.30$; $P > 0.05$). This indicates that wavelet-based quantification with ^{82}Rb and the reference value with $H_2{}^{15}O$ were statistically indistinguishable. The corresponding Bland–Altman plots (Fig. 6) reveal the lack of bias and the reduction in the limits of agreement after the wavelet protocol was applied.

The accuracy of the quantification with the application of wavelet-based noise reduction on ^{82}Rb images and dynamic data can be further shown by the reliability of regional

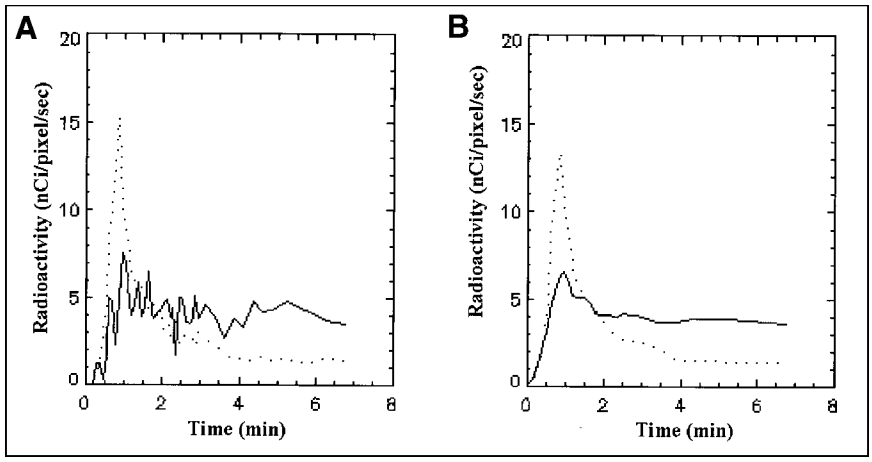

FIGURE 4. Blood (dotted line) and tissue (solid line) time–activity curves of representative ROI after administration of ^{82}Rb before (A) and after (B) wavelet-based noise reduction. Dynamic curves became smoother, yet dynamics in early frames were still preserved.

myocardial perfusion. Without the wavelet approach, the COV of regional flow estimates was large, averaging 75% ± 34% among all of the resting studies (40–64 ROIs per study; total ROIs, 560) and 62% ± 9% among all of the hyperemic studies with ^{82}Rb (40–64 ROIs per study; total ROIs, 448) (Fig. 7). The corresponding COV obtained from the one-compartment model with $H_2{}^{15}O$ was only 13% ± 3% and 17% ± 4% for resting and hyperemic studies, respectively. The wavelet approach markedly reduced the heterogeneity of regional flow estimates with ^{82}Rb to a value of 11% ± 3% for both the resting and the hyperemic studies ($P < 0.001$) (Fig. 7).

DISCUSSION

PET has been used widely to evaluate coronary heart disease and to determine the outcomes of therapeutic interventions (*18*). Quantification of myocardial perfusion by dynamic PET imaging and kinetic models has provided an objective means for measuring the severity and extent of ischemic defects in absolute terms (*19–21*). The use of $^{13}NH_3$ and $H_2{}^{15}O$ with dynamic PET scans has been validated to accurately measure myocardial flow in human subjects (*1–3*). However, the preparation of these two flow tracers requires an on-site cyclotron. Currently, ^{82}Rb is the only generator-produced tracer in clinical use for evaluating myocardial perfusion (*6*). Use of ^{82}Rb increases the flexibility of PET by obviating the need for an on-site cyclotron; its short physical half-life also allows rapid sequential scans (*6,22,23*).

Accurate flow estimates using dynamic images and a compartment model using ^{82}Rb have been difficult to make because of the sensitivity of the estimates to errors and noise (*23*). With the original protocol, the differences between flow estimates with ^{82}Rb and those with $H_2{}^{15}O$ were large, the variation in a normal heart was unacceptably high, and the estimate-to-error ratio of each flow estimate was poor. In addition, estimates with ^{82}Rb became insensitive at high flows (Fig. 5A). These results corroborate our previous findings in animals (*4,5*). Initially, it was believed that the lack of sensitivity at high flows was caused by a fixed

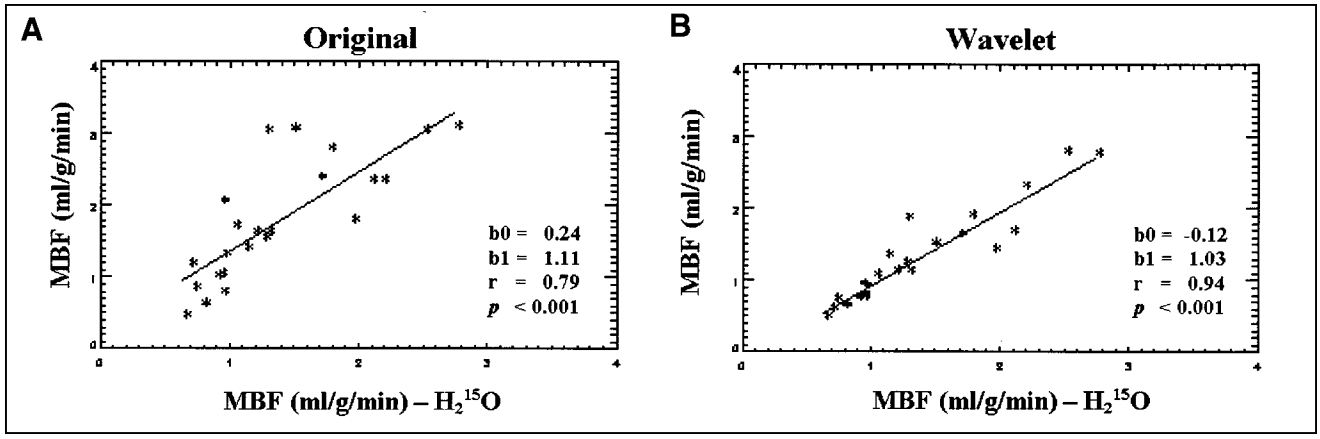

FIGURE 5. Correlation of global flow obtained from human subjects with $H_2{}^{15}O$ (*x*-axis) and ^{82}Rb (*y*-axis) combining resting and hyperemic flows. (A) Original protocol with ^{82}Rb before wavelet-based noise reduction. (B) After wavelet-based noise reduction. Wavelet protocol improved correlation considerably over wide range of flows. MBF = myocardial blood flow; b0 = intercept; b1 = slope of line.

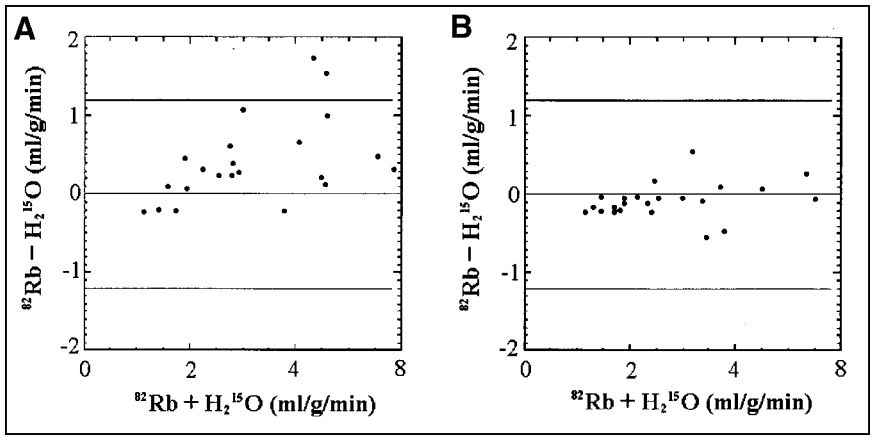

FIGURE 6. Bland–Altman plots between global flows obtained from $H_2{}^{15}O$ studies and ^{82}Rb studies before (A) and after (B) wavelet denoising. Plots show reduction in bias and limits of agreement after wavelet approach.

relationship between flow and extraction fraction during the fitting process. If this were the only reason, decoupling these two parameters would have improved the accuracy of flow estimates. However, a subsequent study that simultaneously estimated flow and rates of transport still revealed significant residuals between flow estimates with ^{82}Rb and the reference values obtained with radiolabeled microspheres (*5*).

The results of this study suggest that the failure to get accurate flow estimates with dynamic PET images with ^{82}Rb is associated with a low signal-to-noise ratio of dynamic data obtained from noisy images and a high error propagation through the kinetic model. The tissue time–activity curve before noise reduction (Fig. 4A) contained fluctuations, the amplitudes of which were about 10%–25% of the average radioactivity in the plateau portion. This signal-to-noise ratio indicates the amount of uncertainty in the observed dynamic curves. The uncertainty was further augmented 5- to 20-fold through the compartment model. Typically, with a point flow estimate of 1.0 mL/g/min, its associated SE might be as high as 0.3–0.6 mL/g/min, significant enough to hamper the accuracy of quantification.

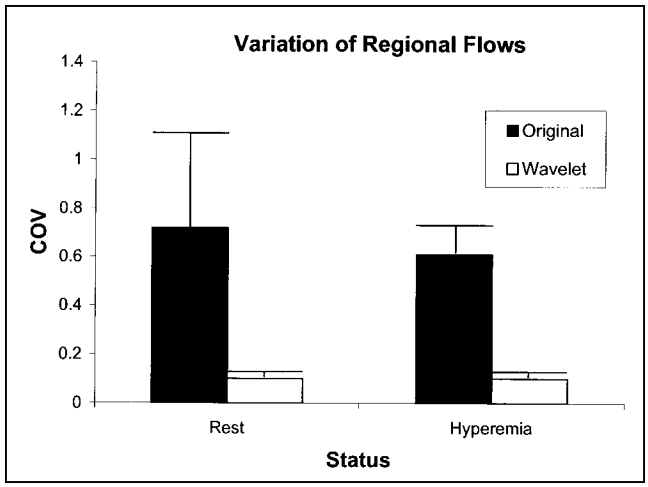

FIGURE 7. COVs, which represent regional variation of flow estimates, were reduced significantly after wavelet process at rest and after dipyridamole.

The kinetic model used in this study contained two compartments and three physiologic parameters (flow, k_1, and k_2). The complex structure of this model describes the behavior of ^{82}Rb in the myocardium but inevitably increases the sensitivity of flow estimates to noise. Therefore, a practical approach should be targeted to reduce the noise of dynamic curves. Selecting a large ROI is one of the intuitive methods to reduce the uncertainty of dynamic data. Klein et al. (*24*) found an inverse relationship between the region size and the regional variation in a dynamic PET study using ^{18}F-FDG to measure cerebral glucose metabolism. Herrero et al. (*5*) segmented ROIs as large as 3–5 cm^3 in canine hearts imaged with ^{82}Rb because blood flow in smaller ROIs could not be assessed accurately. Although the use of larger ROIs increases the statistical stability of dynamic data, it also prevents detection of small regional differences.

The multidimensional wavelet-based noise reduction used in this study avoided this tradeoff. The wavelet approach not only maintained a small region size (0.70–0.85 cm^3) but also faithfully restored the shape of time–activity curves, enhanced the signal-to-noise ratio of dynamic data (Fig. 4B), and improved the accuracy of flow estimates. Although resting flow with ^{82}Rb was slightly lower than the reference value with $H_2{}^{15}O$, the two measurements were statistically identical ($F = 1.30$; $P > 0.05$). However, the slight bias may represent small differences in the current ^{82}Rb model such as the fixed Vd or F_{MM} or a limitation of the denoising approach used.

The linearity and high correlation were preserved over the flow range from 0.45 to 2.75 mL/g/min (Fig. 5B). The lack of sensitivity at high flows with the original protocol (Fig. 5A) actually resulted from the inherent noise that tended to produce an overestimate. The hyperemic flows derived from $H_2{}^{15}O$ and wavelet-denoised ^{82}Rb data in this study are lower than those reported in previous studies (*3*), likely because of different age distributions (*25*,*26*).

The data presented are an average global flow for 40–64 ROIs per subject per scan (i.e., eight segments per short-axis plane × five to eight planes per subject). All segments were averaged to provide one global flow per subject per scan. Although this may smooth the data by creating a global average, as shown in Figure 7, the COV (i.e., the agreement of flow from segment to segment) was high without noise reduction and was reduced to levels that are quite acceptable after noise reduction.

Although many smoothing and filtering methods have been tried to restore underlying biologic signal hidden within multidimensional PET images (*27*), the wavelet approach has multiple advantages over other conventional approaches. First, the wavelet transform provides a built-in local adaptivity. This characteristic successfully preserved the rapid surge of the blood and tissue activity in the early frames (Fig. 4B). Second, the multidimensional wavelet protocol used took into account the geometric position of all ROIs and the temporal relationship among sequential frames and ensured that the reconstructed signal was as smooth as the true underlying function. The common practice that applies kernels or Fourier filters to medical images to improve image quality is an empiric approach, and the best effect is determined visually (*28*). In contrast, the algorithm for wavelet-based noise reduction has a mathematic algorithm to find the near-optimal amount to smooth and, therefore, is an objective approach.

The wavelet denoising approach reduced absolute flow estimated with ^{82}Rb. Although this could be interpreted as a limitation of the wavelet approach, the fact that the denoising process brought flow estimates with ^{82}Rb into line with those obtained with $H_2{}^{15}O$ suggests that the higher flows obtained in unprocessed data were associated with noise. However, underestimation of flow with the approach needs to be evaluated more fully. Studies from our laboratory have shown that wavelet processing does not affect flow estimates with $H_2{}^{15}O$ or $^{13}NH_3$ (*29*).

As noted above, hyperemic flows obtained with $H_2{}^{15}O$ were lower in this study than those in our previous work. The explanation for this is not clear. The healthy subjects in this study were older than those in our previous work, and we have shown that there is a blunted response in the elderly to dipyridamole (*25*). Other possibilities include occult hypercholesterolemia in the healthy volunteers, which is known to blunt the hyperemic response to vasodilatation (*30*), or other methodological issues (difference PET camera or model implementation). The delay between administration of $H_2{}^{15}O$ after dipyridamole, though only 7–8 min, could also lead to a drop-off in coronary flow; however, our previous work (*6*) would suggest that flow after dipyridamole is quite constant for at least 15 min.

CONCLUSION

The results of this study suggest that noninvasive quantification using dynamic PET images with ^{82}Rb accurately measures myocardial perfusion if a multidimensional wavelet-based protocol has appropriately removed noise in the dynamic data. This approach can assess myocardial flow in regions smaller than 1 cm^3 to the accuracy of that achieved with $H_2{}^{15}O$. Therefore, ^{82}Rb can be used to quantify myocardial perfusion in human subjects. The wavelet approach may be applicable to a wide variety of dynamic imaging procedures.

ACKNOWLEDGMENTS

This work was supported in part by grants from the National Heart, Lung, and Blood Institute (grant RO1 HL 46895) and the Jacob and Hilda Blaustein Foundation (grant JB980049).

REFERENCES

1. Choi Y, Huang SC, Hawkins RA, et al. A simplified method for quantification of myocardial blood flow using nitrogen-13-ammonia and dynamic PET. *J Nucl Med*. 1993;34:488–497.
2. Bergmann SR, Fox KA, Rand AL, et al. Quantification of regional myocardial blood flow in vivo with $H_2{}^{15}O$. *Circulation*. 1984;70:724–733.
3. Bergmann SR, Herrero P, Markham J, Weinheimer CJ, Walsh MN. Noninvasive quantitation of myocardial blood flow in human subjects with oxygen-15-labeled water and positron emission tomography. *J Am Coll Cardiol*. 1989;14:639–652.
4. Herrero P, Markham J, Shelton ME, Weinheimer CJ, Bergmann SR. Noninvasive quantification of regional myocardial perfusion with rubidium-82 and positron emission tomography: exploration of a mathematical model. *Circulation*. 1990; 82:1377–1386.
5. Herrero P, Markham J, Shelton ME, Bergmann SR. Implementation and evaluation of a two-compartment model for quantification of myocardial perfusion with rubidium-82 and positron emission tomography. *Circ Res*. 1992;70:496–507.
6. Herrero P, Hartman JJ, Green MA, et al. Regional myocardial perfusion assessed with generator-produced copper-62-PTSM and PET. *J Nucl Med*. 1996;37:1294–1300.
7. Williams BR, Mullani NA, Jansen DE, Anderson BA. A retrospective study of the diagnostic accuracy of a community hospital-based PET center for the detection of coronary artery disease using rubidium-82. *J Nucl Med*. 1994;35: 1586–1592.
8. Huang SC, Williams BA, Krivokapich J, Araujo L, Phelps ME, Schelbert HR. Rabbit myocardial ^{82}Rb kinetics and a compartmental model for blood flow estimation. *Am J Physiol*. 1989;256:H1156–H1164.
9. Mullani NA, Goldstein RA, Gould KL, et al. Myocardial perfusion with rubidium-82. I. Measurement of extraction fraction and flow with external detectors. *J Nucl Med*. 1983;24:898–906.
10. Mullani NA, Gould KL. First-pass measurements of regional blood flow with external detectors. *J Nucl Med*. 1983;24:577–581.
11. Goldstein RA, Mullani NA, Marani SK, Fisher DJ, Gould KL, O'Brien HA Jr. Myocardial perfusion with rubidium-82. II. Effects of metabolic and pharmacologic interventions. *J Nucl Med*. 1983;24:907–915.
12. Kuhle WG, Porenta G, Huang SC, Phelps ME, Schelbert HR. Issues in the quantitation of reoriented cardiac PET images. *J Nucl Med*. 1992;33:1235–1242.
13. Laine A, Koren I. A discrete dyadic wavelet transform for multidimensional feature analysis. In: Akay M, ed. *Time Frequency and Wavelets in Biomedical Signal Processing*. Piscataway, NJ: IEEE; 1998:425–450.
14. Donoho DL, Johnstone IM. Ideal spatial adaptation by wavelet shrinkage. *Biometrika*. 1994;81:425–455.
15. Donoho DL, Johnstone IM. Adapting to unknown smoothness via wavelet shrinkage. *J Am Stat Assoc*. 1995;90:1200–1223.
16. Donoho DL. De-noising by soft-thresholding. *IEEE Trans Inf Theory*. 1995;41: 613–627.
17. Lin JW, Laine A, Bergmann SR. Improving PET-based physiological quantification through wavelet denoising. *IEEE Trans Biomed Eng*. 2001:in press.
18. Bergmann S. Positron emission tomography of the heart. In: Gerson MC, ed. *Cardiac Nuclear Medicine*. 3rd ed. New York, NY: McGraw-Hill; 1997:267–299.
19. Bergmann SR, Sobel BE. Quantification of myocardial perfusion with positron

emission tomography. In: Bergmann SR, Sobel BE, eds. *Positron Emission Tomography of the Heart*. New York, NY: Futura; 1992:97–127.
20. Schelbert HR, Czernin J. Noninvasive quantification of regional myocardial blood flow: assessment of myocardial perfusion reserve and collateral circulation [editorial]. *J Nucl Med*. 1990;31:271–273.
21. Schelbert HR. Consideration of measurements of myocardial blood flow with positron-emission tomography. *Invest Radiol*. 1993;28(suppl 4):S47–S55.
22. Goldstein RA, Mullani N, Wong WH, et al. Positron imaging of myocardial infarction with rubidium-82. *J Nucl Med*. 1986;27:1824–1829.
23. Gould KL. Clinical cardiac PET using generator-produced Rb-82: a review. *Cardiovasc Intervent Radiol*. 1989;12:245–251.
24. Klein GJ, Teng X, Jagust WJ, et al. A methodology for specifying PET VOI's using multimodality techniques. *IEEE Trans Med Imaging*. 1997;16:405–415.
25. Senneff MJ, Geltman EM, Bergmann SR. Noninvasive delineation of the effects of moderate aging on myocardial perfusion. *J Nucl Med*. 1991;32: 2037–2042.
26. Bergmann S, Herrero P, Geltman E. Blunted response of myocardial perfusion to dipyridamole in older adults [letter]. *J Nucl Med.* 1995;36:1426–1427.
27. Herholz K. Non-stationary spatial filtering and accelerated curve fitting for parametric imaging with dynamic PET. *Eur J Nucl Med*. 1988;14:477–484.
28. Healy DM Jr, Lu J, Weaver JB. Two applications of wavelets and related techniques in medical imaging. *Ann Biomed Eng*. 1995;23:637–665.
29. Lin J-W, Laine AF, Akinboboye O, Bergmann SR. Use of wavelet transforms in analysis of time–activity data from cardiac PET. *J Nucl Med.* 2001;42:194–200.
30. Schelbert HR. Positron emission tomography and the changing paradigm in coronary artery disease. *Z Kardiol*. 2000;89(suppl 4):IV55–IV60.

The Journal of NUCLEAR MEDICINE

Quantification of Myocardial Perfusion in Human Subjects Using ^{82}Rb and Wavelet-Based Noise Reduction

Jou-Wei Lin, Robert R. Sciacca, Ru-Ling Chou, Andrew F. Laine and Steven R. Bergmann

J Nucl Med. 2001;42:201-208.

The Journal of Nuclear Medicine is published monthly.
SNMMI | Society of Nuclear Medicine and Molecular Imaging
1850 Samuel Morse Drive, Reston, VA 20190.
(Print ISSN: 0161-5505, Online ISSN: 2159-662X)

SNMMI SOCIETY OF NUCLEAR MEDICINE AND MOLECULAR IMAGING